

Article

Characteristics and Controlling Factors of Groundwater Hydrochemistry in Dongzhi Tableland Area of the Loess Plateau of Eastern Gansu—A Case Study of Ning County Area, North China

Mengnan Zhang ^{1,2} , Shuangbao Han ², Yushan Wang ^{1,2}, Zhan Wang ^{1,3}, Haixue Li ^{1,2}, Xiaoyan Wang ^{1,2}, Jiutan Liu ^{4,*} , Changsuo Li ^{5,*} and Zongjun Gao ⁴

¹ Hebei Center for Ecological and Environmental Geology Research, Hebei GEO University, Shijiazhuang 050031, China

² Center for Hydrogeology and Environmental Geology Survey, China Geological Survey, Baoding 071051, China

³ School of Water Resources and Environment, Hebei GEO University, Shijiazhuang 050031, China

⁴ College of Earth Science and Engineering, Shandong University of Science and Technology, Qingdao 266590, China

⁵ 801 Institute of Hydrogeology and Engineering Geology, Shandong Provincial Bureau of Geology & Mineral Resources, Jinan 250014, China

* Correspondence: ljtsdust@sdust.edu.cn (J.L.); lics120@163.com (C.L.)



Citation: Zhang, M.; Han, S.; Wang, Y.; Wang, Z.; Li, H.; Wang, X.; Liu, J.; Li, C.; Gao, Z. Characteristics and Controlling Factors of Groundwater Hydrochemistry in Dongzhi Tableland Area of the Loess Plateau of Eastern Gansu—A Case Study of Ning County Area, North China. *Water* **2022**, *14*, 3601. <https://doi.org/10.3390/w14223601>

Academic Editors: Alexander Yakirevich and Dedi Liu

Received: 13 October 2022

Accepted: 4 November 2022

Published: 8 November 2022

Publisher's Note: MDPI stays neutral with regard to jurisdictional claims in published maps and institutional affiliations.



Copyright: © 2022 by the authors. Licensee MDPI, Basel, Switzerland. This article is an open access article distributed under the terms and conditions of the Creative Commons Attribution (CC BY) license (<https://creativecommons.org/licenses/by/4.0/>).

Abstract: Groundwater plays an irreplaceable role in all aspects of the Loess Plateau. In this study, the loess phreatic water (LPW) and bedrock phreatic water (BPW) in the Ning County area (NCA) were sampled and analyzed, and the characteristics and controlling factors of groundwater were determined by using statistical analysis, hydrochemical methods, and hydrogeochemical simulation. The results indicated that the groundwater in the NCA was alkaline as a whole, and the average pH values of LPW and BPW were 8.1 and 7.8, respectively. The mean values of TDS concentrations of LPW and BPW were 314.9 mg/L and 675.3 mg/L, and the mean values of TH contents were 194.6 mg/L and 286.6 mg/L, respectively, which were mainly divided into hard fresh water. The Piper diagram illustrated that the hydrochemical type of groundwater in the NCA was mainly the HCO₃-Ca type. The main recharge source of groundwater was atmospheric precipitation, and it was affected by evaporation to a certain extent. The linear relationships of $\delta^{18}\text{O}$ and $\delta^2\text{H}$ of LPW and BPW were $\delta^2\text{H} = 6.998\delta^{18}\text{O} - 3.802$ ($R^2 = 0.98$) and $\delta^2\text{H} = 6.283\delta^{18}\text{O} - 10.536$ ($R^2 = 0.96$), respectively. Hydrochemical analysis indicated that the groundwater in the NCA was mainly controlled by rock weathering and cation exchange. BPW was affected by the dissolution of gypsum. The possible mineral phases were identified on the basis of the main soluble minerals in the aquifer, and hydrogeochemical reverse simulations were performed. The dissolution of calcite, illite, and hornblende, and the precipitation of dolomite, plagioclase, and microcline occurred on both the LPW and BPW pathways.

Keywords: hydrochemical characteristics; major ions; formation mechanism; hydrogeochemical modeling; the Loess Plateau

1. Introduction

Water resources play a pivotal role in human production and life [1–3]. Industrial production, agricultural irrigation, residential life, and ecological maintenance all depend on stable and clean water sources [4–8]. As an important component of water resources, groundwater has the characteristics of stable water quantity and excellent water quality [9]. Groundwater is buried at a certain depth, easy to be exploited and not easily polluted, and has become the preferred source of water for residential and industrial use. Population growth and rapid socio-economic growth have led to increased consumption of

groundwater resources and frequent occurrence of water pollution [10–14]. However, the contradiction between supply and demand of water resources is serious in many regions of the world. Problems such as shortage of groundwater resources, deterioration, and imbalance of groundwater resources limit the sustainable and healthy development of society and economy, having caused serious environmental problems in the past few decades, such as land subsidence, water environment pollution, and water ecosystem degradation [15–18]. To realize the sustainable utilization of regional groundwater resources and promote the coordinated development of the ecological environment and social economy, it is necessary to recognize the hydrochemical characteristics and causes of groundwater resources, as well as to develop and utilize groundwater resources scientifically and rationally [19–21].

The hydrochemical components of groundwater are affected by the long-term action of the environment and continuously interact with the surrounding medium during the migration process, resulting in a series of physical and chemical effects [22–24]. The chemical composition of water contains information such as climate change and the origin of water bodies. Therefore, the environmental quality of groundwater and its ecological functions can be understood by analyzing the chemical composition of water [25–27]. Groundwater under different hydrogeological conditions and human activities has different hydrochemical characteristics. Analyzing the hydrochemical characteristics of groundwater can effectively discriminate the formation process of hydrochemical components and reveal important information such as chemical behavior of elements and chemical weathering intensity in groundwater [28,29]. Therefore, the research on the formation mechanism of groundwater hydrochemistry has important practical significance.

The Chinese Loess Plateau (CLP) is located in the hinterland of China, in the middle reaches of the Yellow River. Affected by the continental monsoon climate, most of its areas belong to arid–semi-arid regions [30]. The CLP is also the region with the most serious soil erosion and the most fragile ecology in China, and the available surface water is very short [31]. The CLP has the widest distribution of loess in the world, and the thickest part of the soil layer is more than 350 m [32]. The deep soil layer forms a huge soil reservoir and groundwater reservoir, providing conditions for the exploitation of groundwater. For a long time, groundwater has become an important source of water supply for agricultural production, industrial development, and residents' domestic use in the CLP. Many researchers have carried out a large number of discussions on the study of groundwater in the Loess Plateau. For example, Li et al. [33] analyzed the hydrogeological conditions and groundwater characteristics, clarified the types and distribution characteristics of freshwater, and revealed the formation mechanism and influencing factors of freshwater on the CLP. Ling et al. [34] studied the isotopic significance of groundwater recharge, retention time, and hydrogeochemical evolution in the CLP of Eastern Gansu. Wang et al. [35] determined the spatial and seasonal variation characteristics and controlling factors of fluorine in natural water on the CLP and assessed its health risks. Xiao et al. [36] analyzed the characteristics and sources of trace elements in river water and well water in the CLP and evaluated water quality and health risks. Zhang et al. [37] studied the hydrochemical processes between surface water and groundwater in the northeastern CLP: implications for water chemistry and environmental evolution in a semi-arid region.

However, the research on the formation mechanism and evolution law of groundwater in the Ning County area (NCA) is relatively limited. Therefore, the purpose of this study was (1) to analyze the hydrochemical characteristics of groundwater in the area, and (2) to clarify the formation mechanism of groundwater hydrochemistry. Statistical analysis, hydrochemical methods, and hydrogeochemical modeling were comprehensively applied in this study, and the research results can provide some reference for the rational utilization of regional groundwater resources and ecological environment protection in the CLP or other similar regions in the world.

2. Study Area

The study area (Figure 1) is located in the middle reaches of the Malian River on the CLP of Eastern Gansu. Geographical coordinates: 35°30′–35°45′ east longitude, 107°45′–108°00′ north latitude. The region is located in the mid-latitude warm temperate zone, with a typical continental monsoon climate. The annual average precipitation is 525.8 mm, the annual maximum precipitation is 827.7 mm (1975), and the annual minimum precipitation is 357.7 mm (1995). The rainfall is mainly concentrated in July–September (Figure 2), and the spatial distribution of rainfall is extremely uneven after the flood season.

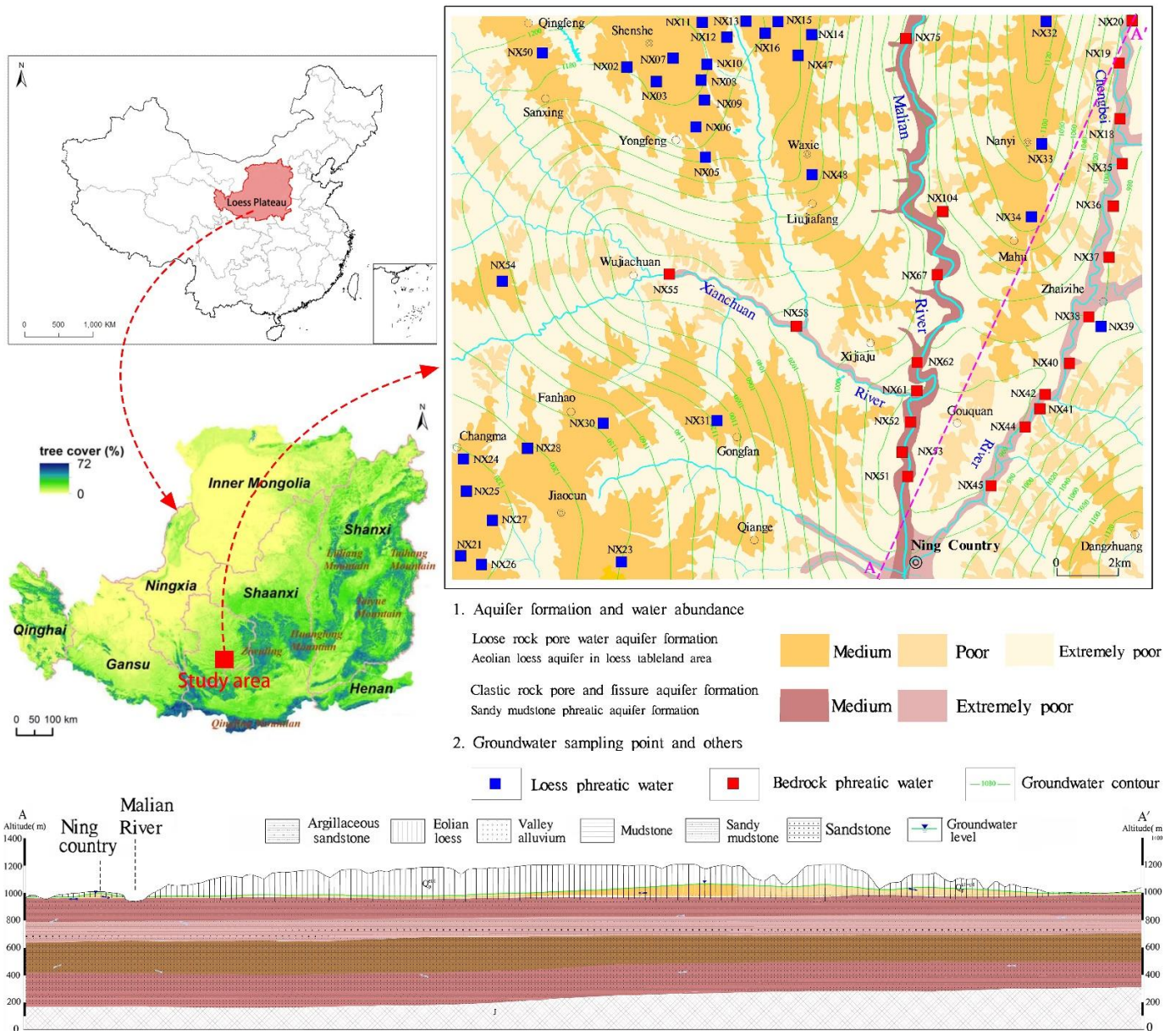


Figure 1. Location map of the study area and groundwater sampling points.

The study area belongs to Longdong Basin, located in the southwest of Ordos Basin, which is a Mesozoic asymmetric syncline basin with a south–north strike, gentle in the east and steep in the west (Figure 3). Its western boundary is the Zhuozi mountain-Pingliang fault zone, the southern part is the Weibei uplift, the eastern boundary is the Ziwu Ridge, and the northern boundary is the Baiyu mountain. Affected by the sedimentation of the CLP and the convoluted structure in Longxi, most of the area is covered by the Quaternary.

In addition, the drilling data in the study area indicate that the strata mainly include the Quaternary Pleistocene loose layer, Cretaceous Huanhe Formation sand mudstone interbed, Cretaceous Luohe Formation medium and coarse sandstone, and Jurassic Anding Formation sand mudstone interbed. Loess and valley sand–gravel layer of loose rock pore aquifer and Huanhe formation bedrock weathering crust pore aquifer formation are the main groundwater exploitation layers in the study area.

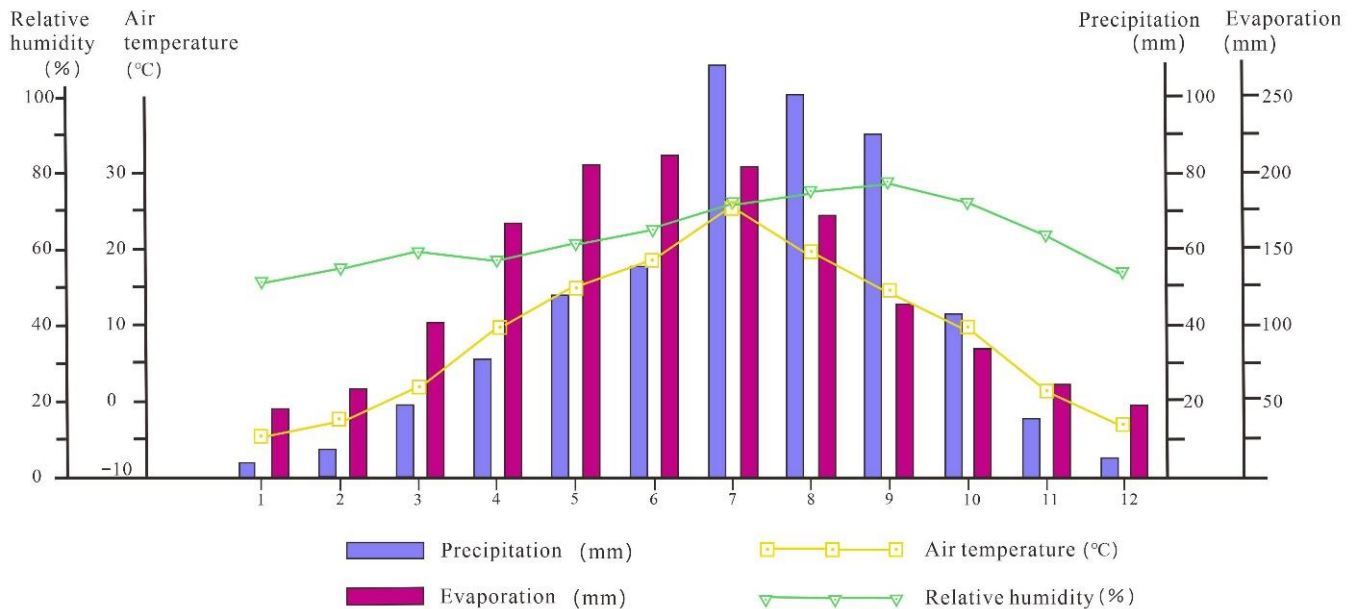


Figure 2. Regional meteorologic map.

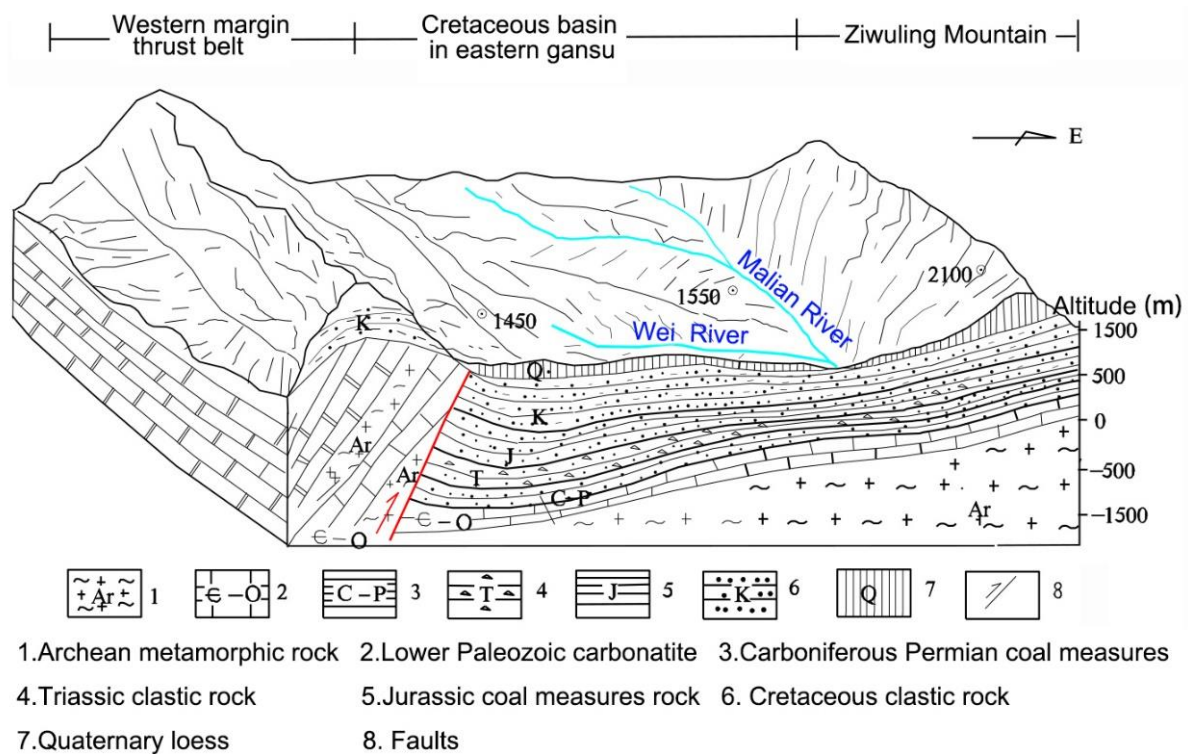


Figure 3. Stereoscopic sketch map of east-west geomorphology and geology in the Longdong basin of eastern Gansu.

The study area (Figure 1) is located in the loess gullied-hilly area in the east of Dongzhi tableland. The overall topography shows that the elevation gradually increases to both sides with the Malian River as the boundary. Quaternary loess is widely distributed in the area, with a thickness of 50–180 m. The region has ravines and gullies criss-cross, undulating terrain, and relatively simple landform, which is mainly divided into three geomorphic types: loess remnant plateau, hilly and gully, and river valley.

The flow direction of groundwater is consistent with the flow direction of surface water and generally flows from the tableland area to the nearby valley area. The recharge area is mainly distributed in the loess tableland, loess hills, and loess ridge area; the discharge area is gullies; and the Malian River valley is the final destination of diving discharge. The dynamic change of phreatic water in the loess tableland has obvious regional and seasonal changes, and the variation amplitude of phreatic water lags behind the precipitation time. The changes of phreatic water level and water volume in the river valley are mainly affected by meteorological and hydrological factors, with obvious seasonal changes. The change of water level lags behind the atmospheric precipitation for 1–2 months. The flow and water level dynamics of bedrock fissure pore phreatic water are mainly controlled by seasonality, and the annual variation range is small, generally 0.5–1.5 m, which is relatively stable.

3. Materials and Methods

3.1. Sampling and Testing

A total of 53 groundwater samples were obtained in this study, including 31 loess phreatic water (LPW) samples and 22 bedrock phreatic water (BPW) samples. The sampling time was June 2018, and the sampling position is shown in Figure 1. LPW is distributed in a large area of loess tableland area in the NCA, and the water-bearing medium is mainly “Lishi loess”. BPW is mainly distributed in the river valley area, with few surface outcrops, and the aquifer is the weathering fissure and interlayer fissure in the surface of the Huanhe Formation. The sampling depth of LPW is mainly between 50 and 100 m, and that of BPW is between 5 and 20 m. All groundwater samples were collected in 2.5 L polyethylene plastic bottles. Bottles were rinsed with the water sample to be taken for more than 3 times before actual sampling. After sampling collection, the bottles were then sealed with sealing film. Groundwater samples were kept refrigerated during transport, and samples were sent to the Gansu geological engineering laboratory for water quality testing analysis within one week of completion of groundwater sampling.

The pH value of groundwater samples was determined by the pH potentiometric method, total dissolved solids (TDS) were determined by drying at 180 °C, and total hardness (TH) was determined by disodium EDTA titration method. The content of cations including K^+ , Na^+ , Ca^{2+} , and Mg^{2+} was determined by atomic absorption spectrometry; the content of anions (Cl^- , SO_4^{2-} , NO_3^- , F^-) was determined by high-performance liquid chromatography; and the concentration of HCO_3^- was determined by titration. Hydrogen (δ^2H) and oxygen ($\delta^{18}O$) stable isotopes were measured using a liquid-water isotope analyzer (CSPC-I26), and Vienna Standard Seawater was used for the determination, using the δ^2H and $\delta^{18}O$ stable isotope content of Vienna standard mean ocean water as the standard. After the water quality test was completed, the ionic charge balance error (%CBE) calculation was carried out. The calculation results showed that the CBE% of all water samples was within the range of $\pm 5\%$, which indicated the reliability of the water quality data.

$$\%CBE = \frac{\sum cation - \sum anion}{\sum cation + \sum anion} \times 100\% \quad (1)$$

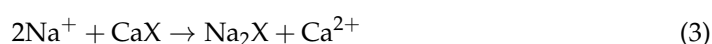
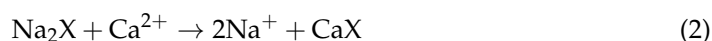
3.2. Geochemical Data Analysis

In this study, descriptive statistics of groundwater hydrochemical data in the Ning County area were firstly carried out by means of statistical analysis, the general characteristics of hydrochemistry were determined, and the hydrochemical types of groundwater were divided by the Piper diagram. Furthermore, using the Gibbs model and the ion ratio

relationship, the genetic mechanism of groundwater was revealed. Finally, the possible hydrogeochemical processes on the groundwater flow path and the amount of mineral transfer were determined on the basis of the hydrogeochemical inverse simulation.

3.3. Cation Exchange

The linear relationship between $Mg^{2+} + Ca^{2+} - HCO_3^- - SO_4^{2-}$ and $K^+ + Na^+ - Cl^-$ was used to identify cation exchange processes (Equations (2) and (3)) in groundwater. If the slope of its linear relationship is -1 , it indicates that cation exchange is an important reaction affecting the hydrochemical characteristics of groundwater [38]. Further, the cation exchange direction can be identified using the chlor-alkali index (CAI) [38,39]. The calculation methods of CAI-1 and CAI-2 are shown in the Equations (4) and (5).



$$CAI - 1 = \frac{Cl^- - Na^+ - K^+}{Cl^-} \quad (4)$$

$$CAI - 2 = \frac{Cl^- - Na^+ - K^+}{HCO_3^- + SO_4^{2-} + CO_3^{2-} + NO_3^-} \quad (5)$$

3.4. Hydrogeochemical Modeling

Hydrogeochemical simulation is an important method to analyze various geochemical interactions in the water–rock interaction system on the basis of equilibrium thermodynamics and chemical kinetics [40,41]. To further analyze the evolution law of groundwater in the study area, two representative groundwater runoff paths were selected, and PHREEQC software (USGS, Virginia State, USA) was used to perform a reverse hydrogeochemical simulation to quantitatively explain the changes of groundwater chemical composition and the main water–rock interactions.

Inverse hydrogeochemical simulations were performed on the basis of PHREEQC software, and the uncertainty of data analysis was set to 0.05. After entering the water quality parameters of the water samples at the initial and terminal points into the software, the SI of minerals and the amount of mineral transfer can be calculated. In the process of operation, considering various factors comprehensively, we adjusted the parameters to obtain the least number of solutions, and finally, we selected the optimal solution.

3.4.1. Saturation Index (SI)

The saturation index [10,26] is used to describe the equilibrium state of minerals and aqueous solutions, referring to the logarithm of the ratio of the ionic activity product (IAP) to the solubility product constant (K_s).

$$SI = \lg \frac{IAP}{K_s} \quad (6)$$

$SI = 0$, $SI > 0$, and $SI < 0$ indicate that the minerals are in the equilibrium state of dissolution–precipitation, supersaturated state, and unsaturated state, respectively.

3.4.2. Mass Balance

The theoretical basis for reverse hydrogeochemical modeling is mass balance. On the basis of the difference of the water chemical composition between the initial point and the terminal point on the groundwater flow path, the possible hydrogeochemical reactions are deduced backward [42,43]. This relationship can be expressed by the mass balance and electron conservation equations, which are as follows:

$$\sum_{n=1}^p a_n b_{n,k} = m_{T,k(\text{terminal point})} - m_{T,k(\text{initial point})} \quad (k = 1, 2, 3) \cdots, j) \quad (7)$$

where a_n represents the moles of phase transfer (dissolution or precipitation) of the n th mineral phase, $b_{n,k}$ represents the stoichiometric number of the k th element of the n th mineral phase, and $m_{T,k}$ represents the total molar concentration of the k th element in the solution (initial or terminal point).

$$\sum_{n=1}^p u_n a_n = \sum_{i=1}^I u_i m_{i(\text{terminal point})} - \sum_{i=1}^I u_i m_{i(\text{initial point})} \quad (8)$$

where u_n represents the effective valence state in the n th mineral phase, u_i represents the effective valence state of the i th component, and m_i represents the molar concentration of the i th component in the solution (initial or terminal point).

4. Results

4.1. Statistical Characteristics of Hydrochemistry

Groundwater is a complex mixed solution, and statistical analysis of its chemical composition can help identify its source and cause [10]. The statistical results of the main chemical components of groundwater are shown in Figure 4. The average pH values of LPW and BPW were 8.1 and 7.8, respectively, indicating that the groundwater in NCA was weakly alkaline as a whole. On average, the dominant cations in LPW and BWP were Na^+ and Ca^{2+} , and the predominant anion was HCO_3^- . In terms of mean value, cations in LPW and BPW were characterized by $\text{Na}^+ > \text{Ca}^{2+} > \text{Mg}^{2+} > \text{K}^+$, while anions were characterized by $\text{HCO}_3^- > \text{SO}_4^{2-} > \text{NO}_3^- > \text{Cl}^- > \text{F}^-$ and $\text{HCO}_3^- > \text{SO}_4^{2-} > \text{Cl}^- > \text{NO}_3^- > \text{F}^-$ (Figure 4), respectively.

TH and TDS in groundwater are important parameters that reflect the quality of water [39,44]. The TH concentrations of LPW and BPW ranged from 77.6 to 906.7 mg/L and 152.1 to 567.5 mg/L, with mean values of 194.6 mg/L and 286.6 mg/L, respectively. The TDS contents of LPW and BPW were in the ranges of 238.2~1142 mg/L and 349.4~1826 mg/L, with averages of 314.9 mg/L and 675.3 mg/L, respectively.

4.2. Hydrochemical Type of Groundwater

The Piper diagram [45] is often used as an effective graphical representation of the chemical composition of water samples in hydrogeological research and is the most widely used diagram in groundwater hydrochemistry research [24,44]. On the basis of the Piper diagram, water chemical types can be divided into four categories (Figure 5), namely, ① $\text{SO}_4\text{-Cl-Ca-Mg}$ type, ② $\text{HCO}_3\text{-Na}$ type, ③ $\text{HCO}_3\text{-Ca}$ type, and ④ $\text{SO}_4\text{-Cl-Na}$ type. The 53 groundwater samples in the NCA were drawn into the Piper diagram, as shown in Figure 4. It can be seen that the groundwater samples were mainly distributed in zone ③, followed by zone ②, indicating that the hydrochemical type of groundwater in the study area was mainly $\text{HCO}_3\text{-Ca}$ type.

4.3. $\delta^2\text{H}$ and $\delta^{18}\text{O}$ Composition Characteristics

Analysis of the $\delta^2\text{H}$ and $\delta^{18}\text{O}$ composition characteristics of groundwater and comparison with the atmospheric precipitation line in the region can be used to determine the source of groundwater recharge [46,47]. The statistical results indicate that the values of $\delta^{18}\text{O}$ and $\delta^2\text{H}$ of LPW were between $-10.85\sim-9.46$ and $-78.40\sim-70.20$, and the mean values were -9.94 and -73.00 , respectively. The values of $\delta^{18}\text{O}$ and $\delta^2\text{H}$ of BPW were in the range of $-12.70\sim-8.70$ and $-92.89\sim-63.34$, and the mean values were -9.88 and -72.95 , respectively. In addition, the linear relationships of the hydrogen and oxygen isotopes of LPW and BPW were $\delta^2\text{H} = 6.998\delta^{18}\text{O} - 3.802$ ($R^2 = 0.98$) and $\delta^2\text{H} = 6.283\delta^{18}\text{O} - 10.536$ ($R^2 = 0.96$), respectively.

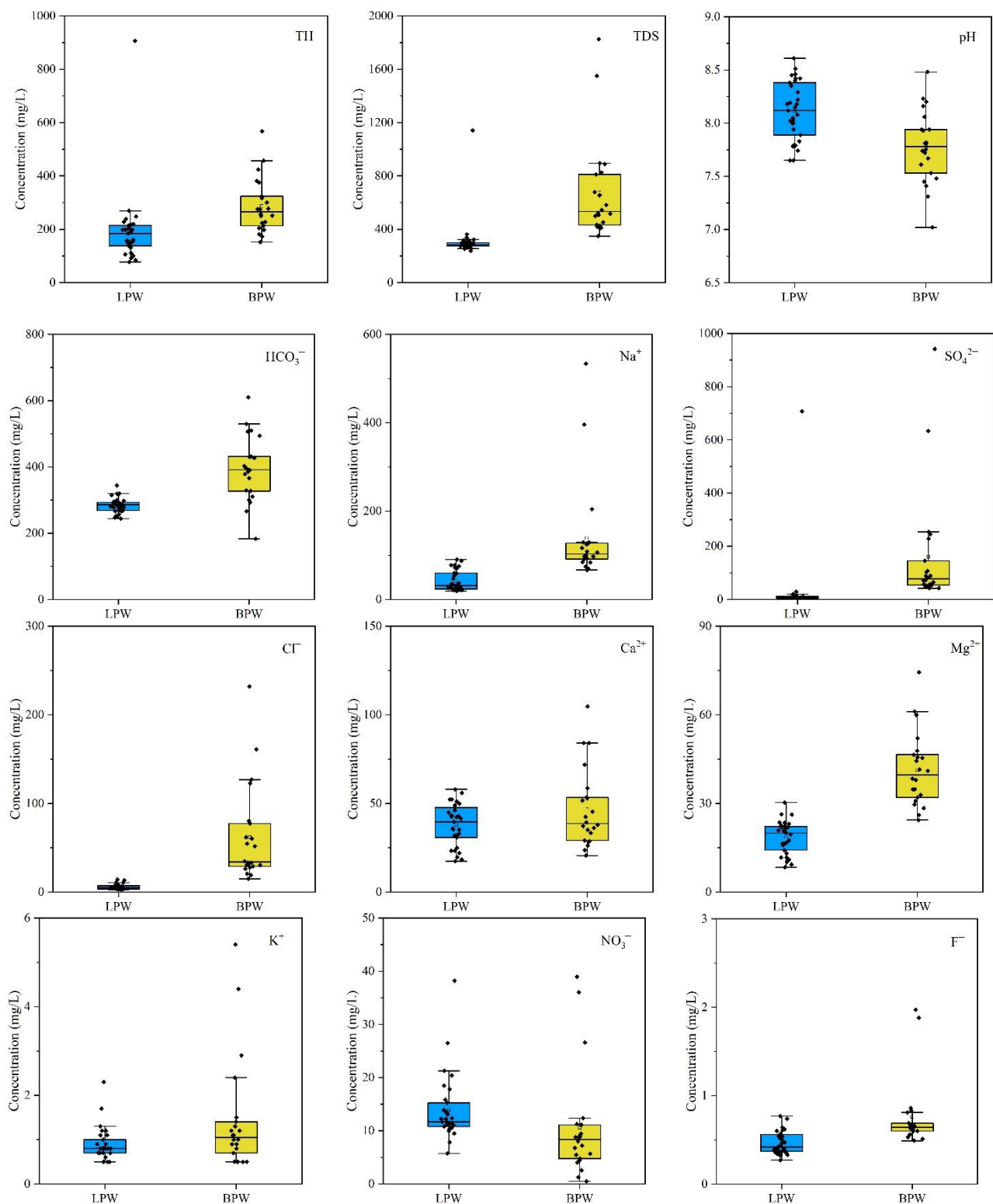


Figure 4. Box diagram of the main chemical components of groundwater.

4.4. Hydrogeochemical Reverse Simulation

4.4.1. Selection of Simulation Path

The precondition for reverse hydrogeochemical simulation is that the initial point and the terminal point are in the upstream and downstream relationship, namely, they are on the same groundwater flow path [42]. It can be seen from Figure 1 that the groundwater

flow direction in the north of the study area was NX32 to NX34, and in the middle valley was along the river (NZ55→NX58). Therefore, according to the location and type of groundwater sampling points, combined with the characteristics of groundwater flow field in the study area (Figure 1), LPW and BPW each selected one profile (LPW path: NX32→NX34, BPW path: NX55→NX58) for simulation. Table 1 illustrates the main chemical components of groundwater samples at the initial and terminal points of different simulation paths.

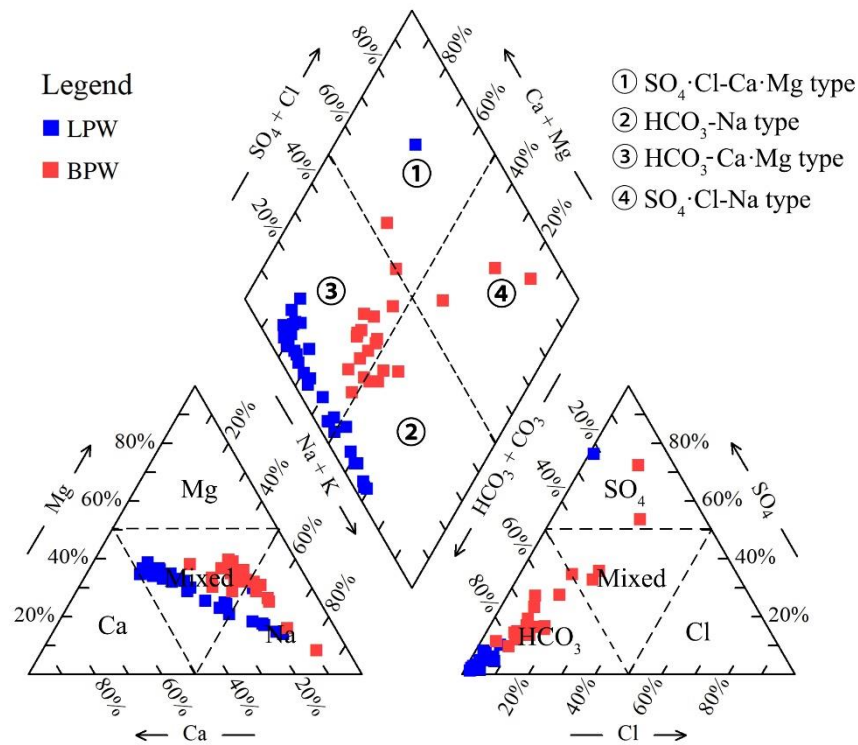


Figure 5. Piper diagram of groundwater hydrochemistry.

Table 1. Main chemical components at the initial point and terminal point of different paths.

	LPW Path (NX32→NX34)		BPW Path (NX55→NX58)	
	Initial Point	Terminal Point	Initial Point	Terminal Point
pH	7.9	8.0	7.0	7.7
TDS (mg/L)	323.5	318.3	581.7	545.8
K ⁺ (mg/L)	0.8	1.1	2.9	0.5
Na ⁺ (mg/L)	21.1	25.3	97.5	129.2
Ca ²⁺ (mg/L)	55.9	52.3	36.2	28.7
Mg ²⁺ (mg/L)	26.2	26.3	45.4	30.8
HCO ₃ ⁻ (mg/L)	278	295	427	393
SO ₄ ²⁻ (mg/L)	11.0	19.7	64.8	103.7
Cl ⁻ (mg/L)	13.5	6.4	51.8	33.3
F ⁻ (mg/L)	0.33	0.34	0.6	0.63
NO ₃ ⁻ (mg/L)	38.2	21.3	26.6	8.0
H ₄ SiO ₄ (mg/L)	28.4	29.2	36.7	25.0

4.4.2. Selection of Possible Mineral Phases

The selection of possible mineral phases is the key to determining the hydrogeochemical reactions that may occur on the groundwater flow path, and is also the core of the mass balance model of water–rock interaction [43]. Many studies have shown that there are two main factors for selecting possible minerals: one is the analysis of the mineral composition in the aquifer, and the main mineral composition in the aquifer should be

given priority; the other is the chemical composition of groundwater and the occurrence conditions of groundwater.

The results of previous studies [48] have indicated that there are differences in the mineral composition and average content of loess soil samples and bedrock rocks in the region. Whole rock mineral X-ray diffraction analysis results showed that the main water-soluble minerals in loess were plagioclase (16.7%), microcline (5.8%), illite (10%), chlorite (13.7%), calcite (8.1%), dolomite (4.9%), and hornblende (3.44%), while the main water-soluble minerals in bedrock rocks were plagioclase (18.6%), microcline (8.8%), illite (10%), chlorite (4.0%), calcite (4.9%), dolomite (6.6%), and gypsum (10%). The possible mineral phases and main reaction equations are shown in Table 2.

Table 2. Possible mineral phases and their reaction equations.

Mineral Name	Reaction Equation
Calcite	$\text{CaCO}_3 = \text{Ca}^{2+} + \text{CO}_3^{2-}$
Dolomite	$\text{CaMg}(\text{CO}_3)_2 = \text{Ca}^{2+} + \text{Mg}^{2+} + 2\text{CO}_3^{2-}$
Gypsum	$\text{CaSO}_4 \cdot 2\text{H}_2\text{O} = \text{Ca}^{2+} + \text{SO}_4^{2-} + 2\text{H}_2\text{O}$
Cation exchange	$2\text{NaX} + \text{Ca}^{2+} = 2\text{Na}^+ + \text{CaX}_2$
Chlorite	$\text{Mg}_5\text{Al}_2\text{Si}_3\text{O}_{10}(\text{OH})_8 + 16\text{H}^+ = 2\text{Al}^{3+} + 6\text{H}_2\text{O} + 3\text{H}_4\text{SiO}_4 + 5\text{Mg}^{2+}$
Illite	$\text{K}_{0.6}\text{Mg}_{0.25}\text{Al}_{2.3}\text{Si}_{3.5}\text{O}_{10}(\text{OH})_2 + 11.2\text{H}_2\text{O} = 0.6\text{K}^+ + 0.25\text{Mg}^{2+} + 2.3\text{Al}(\text{OH})_4^- + 3.5\text{H}_4\text{SiO}_4 + 1.2\text{H}^+$ $2.3\text{Al}(\text{OH})_4^- + 3.5\text{H}_4\text{SiO}_4 + 1.2\text{H}^+$
Plagioclase	$\text{Na}_{0.62}\text{Ca}_{0.38}\text{Al}_{1.38}\text{Si}_{2.62}\text{O}_8 + 5.52\text{H}^+ + 2.48\text{H}_2\text{O} = 1.38\text{Al}^{3+} + 0.38\text{Ca}^{2+} + 2.62\text{H}_4\text{SiO}_4 + 0.62\text{Na}^+$ $+0.38\text{Ca}^{2+} + 2.62\text{H}_4\text{SiO}_4 + 0.62\text{Na}^+$
Hornblende	$\text{Ca}_2\text{Mg}_5\text{Si}_8\text{O}_{22}(\text{OH})_2 + 14\text{H}^+ + 8\text{H}_2\text{O} = 2\text{Ca}^{2+} + 8\text{H}_4\text{SiO}_4 + 5\text{Mg}^{2+}$
Microcline	$\text{KAlSi}_3\text{O}_8 + \text{H}_2\text{O} = \text{K}^+ + \text{Al}(\text{OH})_4^- + 3\text{H}_4\text{SiO}_4$

5. Discussion

5.1. Hydrochemical Characteristics of Groundwater

The order of $\text{Na}^+ > \text{Ca}^{2+} > \text{Mg}^{2+} > \text{K}^+$ existed in the cations in the two types of groundwater, while the anions were slightly different. The relationship of anions in LPW was $\text{HCO}_3^- > \text{SO}_4^{2-} > \text{NO}_3^- > \text{Cl}^- > \text{F}^-$, and the order of anions in BWP $\text{HCO}_3^- > \text{SO}_4^{2-} > \text{Cl}^- > \text{NO}_3^- > \text{F}^-$. When we compared the content of main chemical components in LPW and BPW (Figure 4), except for the fact that the pH value in LPW was higher than that in BPW, we found that other components were lower than BPW.

According to the classification [39,44] of TH and TDS (Figure 6a), the groundwater in Ning County was mainly divided into two categories: soft fresh water (18.9%) and hard fresh water (75.5%). In addition, one LPW sample and two BPW samples belonged to hard brackish water. All BWP samples were classified as hard water, while the proportion of LPW samples classified as hard water was 67.7%. The total ionic salinity (TIS) of LPW and BPW were in the range of 8.58–38.86 meq/L and 12.44–54.29 meq/L (Figure 6b), respectively. In addition, the $\text{HCO}_3\text{-Ca}$ type was the predominant type of groundwater in the study area, indicating that the hydrochemical characteristics of groundwater may be influenced by the dissolution of carbonate rock minerals.

5.2. Hydrochemical Genetic Mechanism

5.2.1. Rock Weathering

The Gibbs diagram [49] divides the main formation mechanisms that control water chemistry into three categories: precipitation, evaporation, and rock weathering. At present, the Gibbs graphical model is widely used to identify the controlling factors of groundwater hydrochemical characteristics [12,29]. The 53 groundwater samples in the NCA were projected onto the Gibbs map, as shown in Figure 7. It can be seen that the water sample points were mainly located in the rock weathering control area, that is, rock weathering was found to be the main formation mechanism of groundwater hydrochemistry in the NCA.

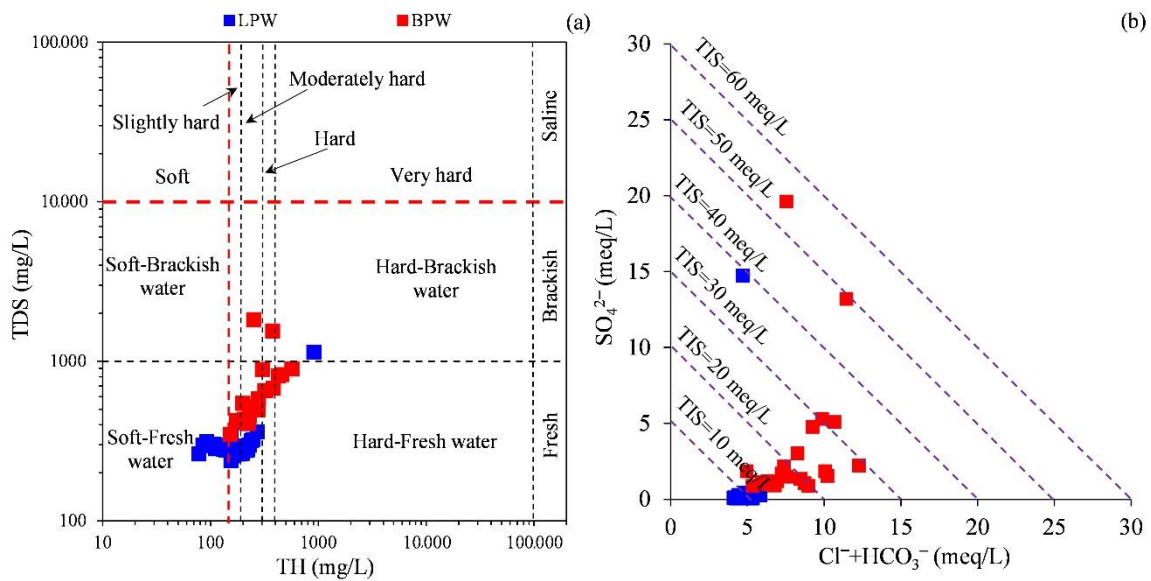


Figure 6. Scatter diagram of TH vs. TDS (a) and SO_4^{2-} vs. $Cl^- + HCO_3^-$ (b) of groundwater samples in the study area.

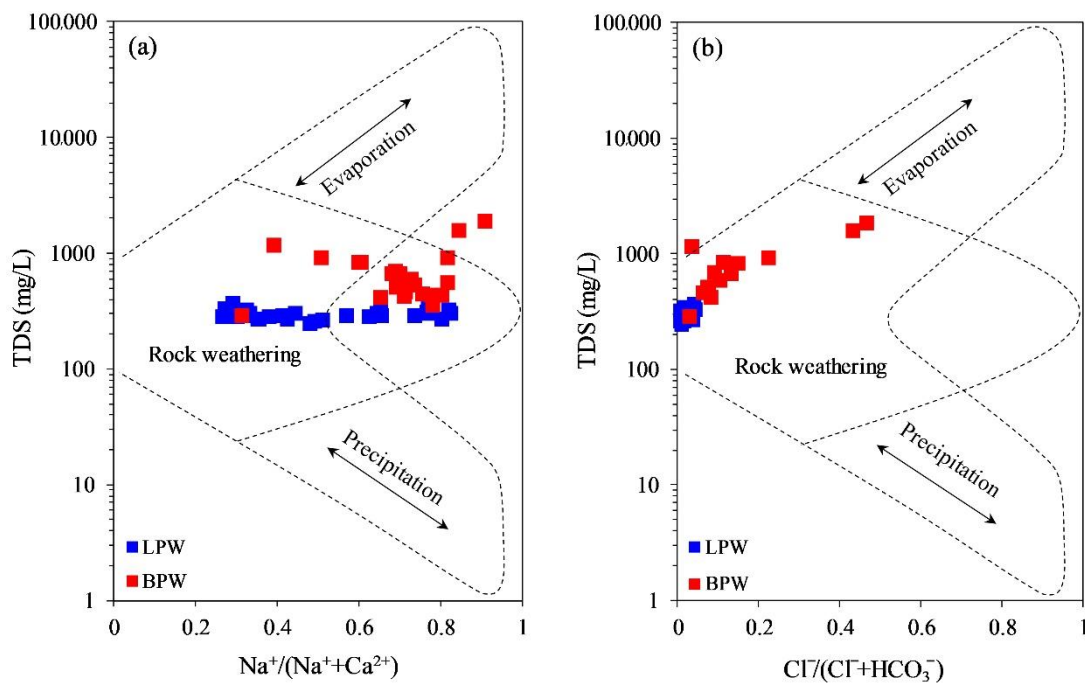


Figure 7. Gibbs diagram of groundwater hydrochemistry TDS vs. $Na^+ / (Na^+ + Ca^{2+})$ (a) TDS vs. $Cl^- / (Cl^- + HCO_3^-)$ (b).

5.2.2. Mineral Dissolution

The main ion ratio relationship in groundwater can be used to further determine the rock weathering source type and mineral dissolution [22,24]. The Na^+ to Cl^- ratio relationship can be used to determine the effect of halite dissolution on groundwater chemistry, since the dissolution of halite produces equal amounts of Na^+ and Cl^- (Equation (9)). Figure 8a illustrates that all groundwater samples in the Ning County area were distributed on the right side of the line $Na^+ / Cl^- = 1$, namely, $Na^+ / Cl^- > 1$ in groundwater, indicating that the dissolution of halite was not the main source of Na^+ and Cl^- in groundwater in

the area. In addition, excess Na^+ may originate from other hydrogeochemical processes such as dissolution of silicate minerals or cation exchange.

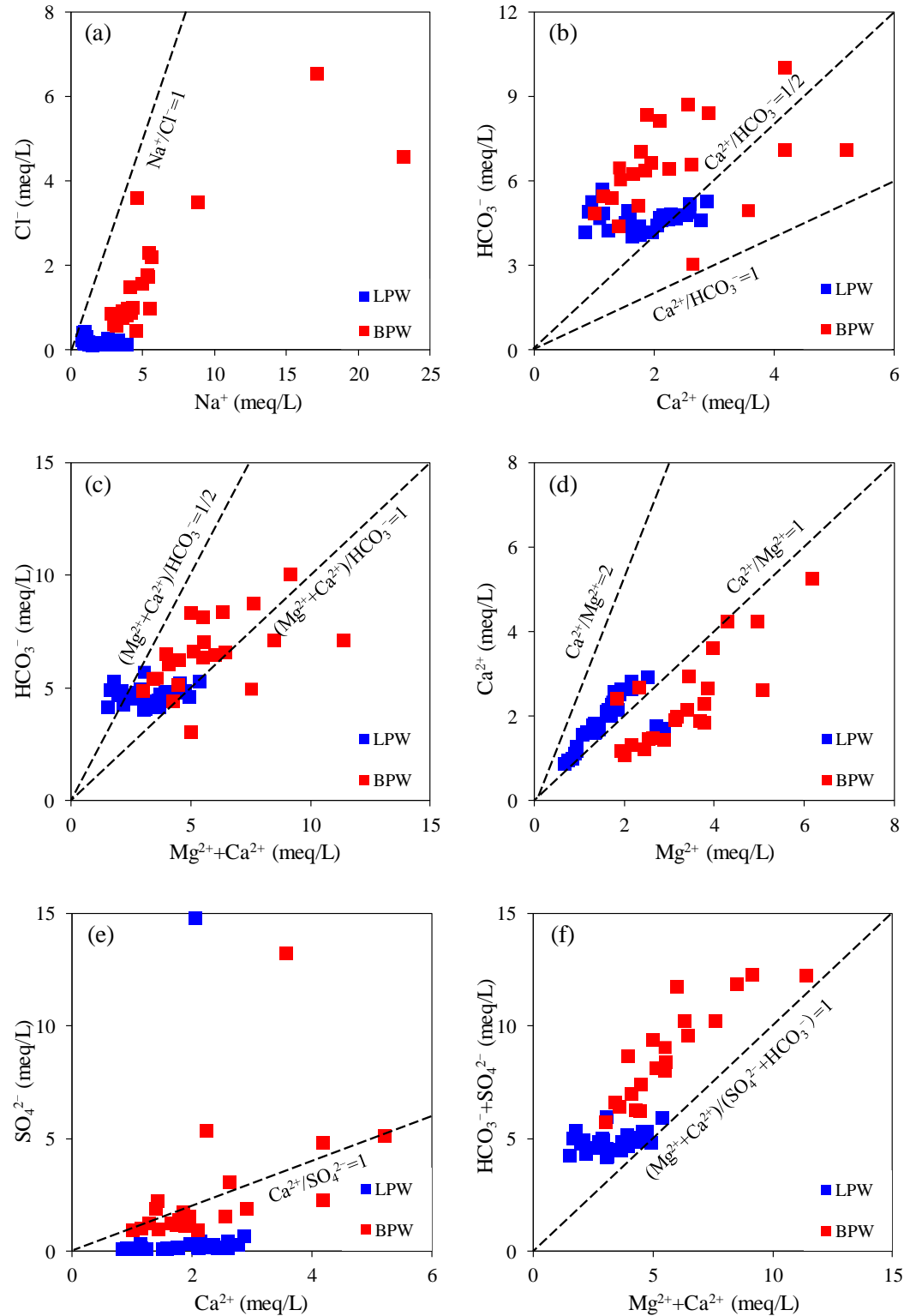
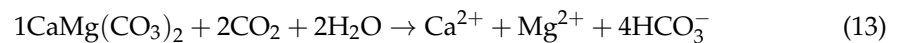
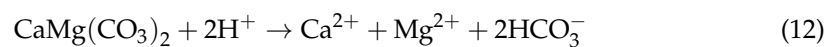
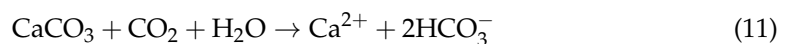
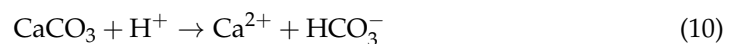


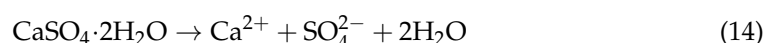
Figure 8. The relationship between the ion ratios of the main chemical components in the groundwater. Na^+ vs. Cl^- (a), Ca^{2+} vs. HCO_3^- (b), $\text{Mg}^{2+} + \text{Ca}^{2+}$ vs. HCO_3^- (c), Mg^{2+} vs. Ca^{2+} (d), SO_4^{2-} vs. Ca^{2+} (e) and $\text{Mg}^{2+} + \text{Ca}^{2+}$ vs. $\text{SO}_4^{2-} + \text{HCO}_3^-$ (f).

The ratio relationship between Ca^{2+} , Mg^{2+} , and HCO_3^- is widely used to determine the influence of the dissolution of carbonate minerals (calcite and dolomite) in groundwater on hydrochemical characteristics [6,39]. As shown in the Figure 8b, some water samples were distributed near the $\text{Ca}^{2+}/\text{HCO}_3^- = 1/2$ line or between the $\text{Ca}^{2+}/\text{HCO}_3^- = 1/2$ line and $\text{Ca}^{2+}/\text{HCO}_3^- = 1$ line, indicating that the chemical characteristics of groundwater in the study area are affected by the dissolution of calcite (Equations (10) and (11)). Furthermore, most of the water samples were distributed near the line $\text{Ca}^{2+} + \text{Mg}^{2+}/\text{HCO}_3^- = 1$ or between the line $\text{Ca}^{2+} + \text{Mg}^{2+}/\text{HCO}_3^- = 1$ and the line $\text{Ca}^{2+} + \text{Mg}^{2+}/\text{HCO}_3^- = 1/2$ (Figure 8c), illustrating that the dissolution of dolomite (Equations (12) and (13)) is an important process affecting the chemical characteristics of groundwater in the study area.



The ratio of $\text{Ca}^{2+}/\text{Mg}^{2+}$ is often used to reveal the source of Ca^{2+} and Mg^{2+} in groundwater [50]. $\text{Ca}^{2+}/\text{Mg}^{2+} = 1$ indicates that it comes from the dissolution of dolomite, while if $1 < \text{Ca}^{2+}/\text{Mg}^{2+} < 2$, it means that there is more dissolution of calcite. $\text{Ca}^{2+}/\text{Mg}^{2+} > 2$ indicates that more Ca^{2+} is provided by the dissolution of silicate minerals or gypsum [50]. As shown in Figure 8d, the LPW samples were mainly distributed between $\text{Ca}^{2+}/\text{Mg}^{2+} = 1$ and $\text{Ca}^{2+}/\text{Mg}^{2+} = 2$, indicating that the Ca^{2+} in LPW mainly originated from the dissolution of calcite. In addition, the BPW samples were mainly concentrated below the line of $\text{Ca}^{2+}/\text{Mg}^{2+} = 1$, indicating that the dissolution of dolomite or Mg-rich carbonate minerals had an important influence on the chemical composition of the BPW.

The dissolution of gypsum may be one of the important sources of SO_4^{2-} in groundwater in a region. If gypsum is the only source of Ca^{2+} and SO_4^{2-} in groundwater, the ratio of Ca^{2+} to SO_4^{2-} should be 1 (Equation (13)). As shown in Figure 8e, most of the BPW samples were distributed close to the $\text{Ca}^{2+}/\text{SO}_4^{2-} = 1$ line, while the LPW samples deviated from the $\text{Ca}^{2+}/\text{SO}_4^{2-} = 1$ line, indicating that the dissolution of gypsum had a more significant contribution to the chemical characteristics of the BPW. In addition, the oxidation of pyrite or other sulfur-bearing minerals may also be a source of SO_4^{2-} in groundwater [8]. However, the Cretaceous strata in the study area were generally a set of complex sediments under arid and semi-arid climate conditions, in which the upper part of sandstone and mudstone of the Huanhe formation was mostly sandwiched with a salt marsh facies gypsum layer, with high salt content and being rich in gypsum, sodium sulfate, halite, and other evaporite minerals [51]. Thus, the main source of SO_4^{2-} in the groundwater of the NCA is the dissolution of gypsum and other sulfate minerals. The relationship between $\text{Mg}^{2+} + \text{Ca}^{2+}$ and $\text{HCO}_3^- + \text{SO}_4^{2-}$ is also often used to explain the contribution of the weathering of carbonate and silicate and the dissolution of gypsum to groundwater hydrochemical characteristics [50]. As shown in Figure 8f, the groundwater sample points were mainly distributed in the upper part of the line $(\text{Mg}^{2+} + \text{Ca}^{2+})/(\text{HCO}_3^- + \text{SO}_4^{2-}) = 1$, indicating that the weathering of carbonate and the dissolution of gypsum were important processes that affect the chemical composition of groundwater in the NCA.



5.2.3. Cation Exchange

In general, cation exchange may also be an important hydrogeochemical reaction in a regional groundwater system that affects the chemical composition of groundwater [16,38]. As shown in Figure 9a, groundwater sample points in Ning County were all distributed along the $x/y = -1$ line, and only one LPW sample deviated from the $x/y = -1$ line, suggesting that cation exchange is an important hydrochemical process in the groundwater

system in the region. If the CAI value is greater than 0, it indicates that reverse cation exchange has occurred, resulting in the exchange of Na^+ in groundwater with Ca^{2+} in the aquifer (Equation (2)). If the Ca^{2+} in groundwater is exchanged with Na^+ in the aquifer, direct cation exchange occurs (Equation (3)), and the value of CAI is less than 0. Figure 9b illustrates that the calculated CAI values of the water samples were all less than 0, indicating that direct cation exchange occurred in the groundwater system in the NCA.

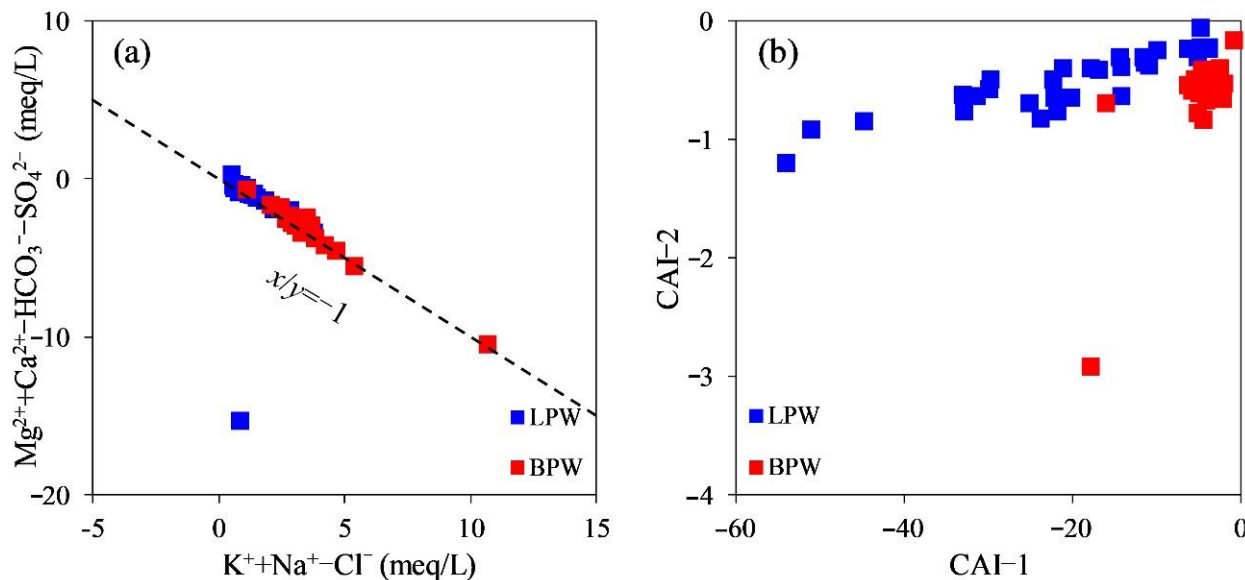


Figure 9. Diagrams of (a) $\text{K}^+ + \text{Na}^+ - \text{Cl}^-$ vs. $\text{Mg}^{2+} + \text{Ca}^{2+} - \text{HCO}_3^- - \text{SO}_4^{2-}$ and (b) CAI-1 vs. CAI-2.

5.3. Analysis of Groundwater Recharge Sources

The $\delta^2\text{H}$ and $\delta^{18}\text{O}$ data of groundwater samples in the study area were compared and analyzed with the Global Meteoric Water Line (GMWL) and the Local Meteoric Water Line (LMWL), as shown in Figure 10. Generally, the water sample points were distributed close to the atmospheric precipitation line, indicating that the main source of the water body was atmospheric precipitation. The GMWL ($\delta\text{D} = 8\delta^{18}\text{O} + 10$) in Figure 10 was obtained by Craig [52] in 1961. In addition, the LMWL in this study adopted the atmospheric precipitation line ($\delta\text{D} = 8.10\delta^{18}\text{O} + 6.97$) in the Pingliang area [53], which was close to the study area. It can be seen from Figure 10 that the groundwater sample points in the study area were mainly distributed near the lower part of the GMWL and along the LMWL as a whole, indicating that the main recharge source of groundwater in the region was atmospheric precipitation, which is affected by evaporation to a certain extent.

5.4. Hydrogeochemical Simulation Results

5.4.1. Saturation Index (SI)

The saturation indices and charge balance coefficients of minerals in groundwater at starting points on different simulation paths are shown in Table 3. Charge balance is a fundamental condition for performing reverse hydrogeochemical simulations. Table 4 illustrates that the charge balance coefficients of the water samples on the groundwater flow path were all close to 0, which indicates that the charges were essentially balanced. Table 3 indicates that there was a difference in the SI between the initial point and terminal point. The SI was less than 0, indicating that these minerals in the groundwater did not reach a saturated state, and that these minerals have a tendency to dissolve. The SI was greater than 0, indicating that it is in a supersaturated state and there is a tendency for precipitation to occur.

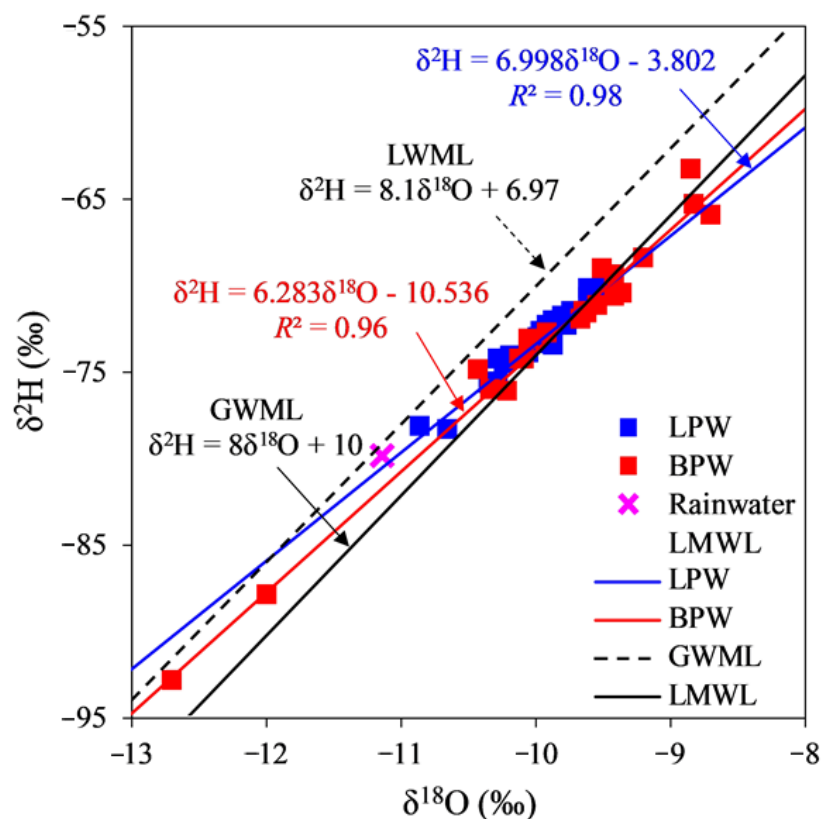


Figure 10. $\delta^2\text{H}-\delta^{18}\text{O}$ relationship diagram of groundwater.

Table 3. Calculated mineral saturation index and charge balance coefficient.

	LPW Path (NX32→NX34)		BPW Path (NX55→NX58)	
	Initial Point	Terminal Point	Initial Point	Terminal Point
Calcite	0.68	0.80	-0.24	0.26
Dolomite	1.39	1.65	-0.04	0.90
Gypsum	-2.66	-2.44	-2.16	-2.04
Chlorite	-0.22	0.81	-6.00	-2.15
Illite	-1.23	-1.28	0.50	-1.31
Plagioclase	9.16	9.21	9.72	9.35
Hornblende	7.22	9.49	-3.11	3.52
Microline	-2.21	-2.06	-1.36	-2.61
Charge balance coefficient	-2.5×10^{-4}	-5.88×10^{-4}	-1.48×10^{-3}	-1.35×10^{-3}

Table 4. Mineral transfer mass on the LPW path and BPW path.

	Mineral Transfer Mass (mol/L)	
	LPW Path	BPW Path
Calcite	8.197×10^{-4}	3.667×10^{-3}
Dolomite	-2.658×10^{-4}	-2.826×10^{-3}
Gypsum	/	3.297×10^{-4}
Chlorite	-2.170×10^{-4}	2.850×10^{-4}
Illite	1.231×10^{-4}	4.899×10^{-4}
Plagioclase	-1.208×10^{-4}	-9.721×10^{-4}
Microline	-7.311×10^{-4}	-3.554×10^{-4}
Hornblende	2.127×10^{-4}	1.233×10^{-4}
NaX	1.150×10^{-3}	2.537×10^{-3}
CaX ₂	-5.750×10^{-4}	-1.269×10^{-3}

5.4.2. Mineral Transfer Mass

By using the PHREEQC software, the amount of mineral transfer mass on the simulated path was calculated. Mineral transfer masses greater than 0 or less than 0 represent mineral dissolution and precipitation, respectively. It can be seen from Table 4 that the dissolution of calcite, illite, and hornblende, as well as the precipitation of dolomite, plagioclase, and microcline occurred on both the LPW and BPW simulation paths. In addition, cation exchange occurred on both paths, and the Na^+ in the aquifer was replaced with Ca^{2+} in the groundwater. The dissolution of gypsum and chlorite also occurred on the BWP path, while the precipitation of chlorite occurred on the LPW path. On different groundwater flow paths, the hydrogeochemical reactions of mineral transfer mass were different, which was the result of the combined effects of the lithology, geology, and hydrogeological conditions of the aquifer and its surrounding physical, chemical, and biological environments.

5.5. Suggestions for Regional Groundwater Research

This study analyzed the chemical characteristics and controlling factors of groundwater in the NCA, and the research results can provide reference for the development and utilization of regional groundwater resources. However, the data from this study are only from a sampling period, and future studies should carry out sampling for different periods, depths, and types of groundwater in order to obtain more water quality data. In addition, other chemical components in groundwater such as trace elements, heavy metals, and organic matter should also be analyzed in order to enrich the results of regional groundwater-related studies and provide more comprehensive support for the development and utilization of groundwater resources.

6. Conclusions

The study of groundwater hydrochemistry is helpful for the rational development, utilization, and management of groundwater resources in a region, and can also provide a reference for similar regions in the world. To understand the hydrochemical characteristics and formation mechanism of groundwater in the NCA of the Loess Plateau, the LPW and BPW were sampled and analyzed, respectively, and the following main conclusions were obtained:

- (1) The groundwater of NCA was weakly alkaline as a whole, mainly classified as hard fresh water, and $\text{HCO}_3\text{-Ca}$ was the dominant hydrochemical type. Except for pH, the concentrations of major chemical components in BPW were higher than those in LPW.
- (2) $\delta^2\text{H}$ and $\delta^{18}\text{O}$ analysis illustrated that the main recharge source of groundwater in NCA was atmospheric precipitation and was affected by evaporation. The linear relationships of the $\delta^2\text{H}$ and $\delta^{18}\text{O}$ of LPW and BPW were $\delta^2\text{H} = 6.998\delta^{18}\text{O} - 3.802$ ($R^2 = 0.98$) and $\delta^2\text{H} = 6.283\delta^{18}\text{O} - 10.536$ ($R^2 = 0.96$), respectively.
- (3) The main controlling factors of LPW and BPW in the study area were rock weathering and cation exchange. Ca^{2+} , Mg^{2+} , and HCO_3^- in groundwater mainly originated from the dissolution of calcite and dolomite. In addition, the dissolution of gypsum also had a significant effect on the water chemical composition of BPW.
- (4) Hydrogeochemical inverse simulations indicated that cation exchange; the dissolution of calcite, illite, and hornblende; and the precipitation of dolomite, plagioclase, and microcline occurred on both the LPW and BPW pathways. In addition, the dissolution of gypsum and chlorite also occurred on the BWP path, and the precipitation of chlorite occurred on the LPW path.

Author Contributions: Conceptualization, M.Z., J.L., C.L. and Z.G.; Methodology, M.Z., J.L., C.L., and Z.G.; Software, S.H., Y.W., Z.W., H.L. and X.W.; Validation, M.Z., J.L., C.L. and Z.G.; Formal Analysis, M.Z., J.L., C.L. and Z.G.; Investigation, S.H., Y.W., Z.W., H.L. and X.W.; Resources, S.H., Y.W., Z.W., H.L. and X.W.; Data Management, S.H., Y.W., Z.W., H.L. and X.W.; Writing—Manuscript Preparation, M.Z., J.L., C.L. and Z.G.; Writing—Review and Editing, M.Z., J.L., C.L. and Z.G.; Visualization, M.Z., J.L., C.L. and Z.G.; Supervision, S.H., Y.W., Z.W., H.L. and X.W.; Project Management, M.Z.; Funding Acquisition, M.Z. All authors have read and agreed to the published version of the manuscript.

Funding: The study involved in this paper was supported by the Open Project Program of the Hebei Center for Ecological and Environmental Geology Research (no. JSYF-202204); 1:50,000 Hydrogeological Survey in the Old Revolutionary Areas of Shanxi, Gansu, and Ningxia (no. DD20160288); and Investigation and Monitoring of Hydrogeology and Water Resources in Key Areas of Yellow River Basin (no. DD20221754). We thank the editors and anonymous reviewers for their valuable suggestions on the manuscript.

Institutional Review Board Statement: Not applicable.

Informed Consent Statement: Not applicable.

Data Availability Statement: Not applicable.

Conflicts of Interest: The authors declare no conflict of interest.

References

1. Jaydhar, A.K.; Pal, S.C.; Saha, A.; Islam, A.R.M.T.; Ruidas, D. Hydrogeochemical evaluation and corresponding health risk from elevated arsenic and fluoride contamination in recurrent coastal multi-aquifers of eastern India. *J. Clean. Prod.* **2022**, *369*, 133150. [[CrossRef](#)]
2. Pal, S.C.; Ruidas, D.; Saha, A.; Islam, A.R.M.T.; Chowdhuri, I. Application of novel data-mining technique based nitrate concentration susceptibility prediction approach for coastal aquifers in India. *J. Clean. Prod.* **2022**, *346*, 131205. [[CrossRef](#)]
3. Ruidas, D.; Pal, S.C.; Saha, A.; Chowdhuri, I.; Shit, M. Hydrogeochemical characterization based water resources vulnerability assessment in India's first Ramsar site of Chilka lake. *Mar. Pollut. Bull.* **2022**, *184*, 114107. [[CrossRef](#)] [[PubMed](#)]
4. Ruidas, D.; Pal, S.C.; Islam, A.R.M.T.; Saha, A. Characterization of groundwater potential zones in water-scarce hardrock regions using data driven model. *Environ. Earth Sci.* **2021**, *80*, 809. [[CrossRef](#)]
5. Vaiphei, S.P.; Kurakalva, R.M. Hydrochemical characteristics and nitrate health risk assessment of groundwater through seasonal variations from an intensive agricultural region of upper Krishna River basin, Telangana, India. *Ecotoxicol. Environ. Saf.* **2021**, *213*, 112073. [[CrossRef](#)]
6. Wang, X.; Zheng, W.; Tian, W.; Gao, Y.; Wang, X.; Tian, Y.; Li, J.; Zhang, X. Groundwater hydrogeochemical characterization and quality assessment based on integrated weight matter-element extension analysis in Ningxia, upper Yellow River, northwest China. *Ecol. Indic.* **2022**, *135*, 108525. [[CrossRef](#)]
7. Keum, G.; Kim, Y.; Lee, K.-S.; Jeong, J. The geochemistry and isotopic compositions of the Nakdong River, Korea: Weathering and anthropogenic effects. *Environ. Monit. Assess.* **2022**, *194*, 487. [[CrossRef](#)]
8. Fuoco, I.; De Rosa, R.; Barca, D.; Figoli, A.; Gabriele, B.; Apollaro, C. Arsenic polluted waters: Application of geochemical modelling as a tool to understand the release and fate of the pollutant in crystalline aquifers. *J. Environ. Manag.* **2022**, *301*, 113796. [[CrossRef](#)]
9. Li, C.; Gao, Z.; Chen, H.; Wang, J.; Liu, J.; Li, C.; Teng, Y.; Liu, C.; Xu, C. Hydrochemical analysis and quality assessment of groundwater in southeast North China Plain using hydrochemical, entropy-weight water quality index, and GIS techniques. *Environ. Earth Sci.* **2021**, *80*, 523. [[CrossRef](#)]
10. Liu, J.; Peng, Y.; Li, C.; Gao, Z.; Chen, S. Characterization of the hydrochemistry of water resources of the Weibei Plain, Northern China, as well as an assessment of the risk of high groundwater nitrate levels to human health. *Environ. Pollut.* **2021**, *268*, 115947. [[CrossRef](#)]
11. Peng, H.; Yang, W.; Ferrer, A.S.N.; Xiong, S.; Li, X.; Niu, G.; Lu, T. Hydrochemical characteristics and health risk assessment of groundwater in karst areas of southwest China: A case study of Bama, Guangxi. *J. Clean. Prod.* **2022**, *341*, 130872. [[CrossRef](#)]
12. Xiao, Y.; Hao, Q.; Zhang, Y.; Zhu, Y.; Yin, S.; Qin, L.; Li, X. Investigating sources, driving forces and potential health risks of nitrate and fluoride in groundwater of a typical alluvial fan plain. *Sci. Total Environ.* **2022**, *802*, 149909. [[CrossRef](#)] [[PubMed](#)]
13. Saha, A.; Pal, S.C.; Chowdhuri, I.; Roy, P.; Chakraborty, R. Effect of hydrogeochemical behavior on groundwater resources in Holocene aquifers of moribund Ganges Delta, India: Infusing data-driven algorithms. *Environ. Pollut.* **2022**, *314*, 120203. [[CrossRef](#)] [[PubMed](#)]
14. Schwarzenbach, R.P.; Egli, T.; Hofstetter, T.B.; Von Gunten, U.V.; Wehrli, B. Global Water Pollution and Human Health. *Annu. Rev. Environ. Resour.* **2010**, *35*, 109–136. [[CrossRef](#)]
15. Misstear, B.; Vargas, C.R.; Lapworth, D.; Ouedraogo, I.; Podgorski, J. A global perspective on assessing groundwater quality. *Hydrogeol. J.* **2022**. [[CrossRef](#)]
16. Mohammed, A.M.; Refaee, A.; El-Din, G.K.; Harb, S. Hydrochemical characteristics and quality assessment of shallow groundwater under intensive agriculture practices in arid region, Qena, Egypt. *Appl. Water Sci.* **2022**, *12*, 92. [[CrossRef](#)]
17. Lapworth, D.; Boving, T.; Kremer, D.; Kebede, S.; Smedley, P. Groundwater quality: Global threats, opportunities and realising the potential of groundwater. *Sci. Total Environ.* **2022**, *811*, 152471. [[CrossRef](#)]
18. Fuoco, I.; Marini, L.; De Rosa, R.; Figoli, A.; Gabriele, B.; Apollaro, C. Use of reaction path modelling to investigate the evolution of water chemistry in shallow to deep crystalline aquifers with a special focus on fluoride. *Sci. Total Environ.* **2022**, *830*, 154566. [[CrossRef](#)]

19. Liu, Y.; Engel, B.A.; Flanagan, D.C.; Gitau, M.W.; McMillan, S.K.; Chaubey, I. A review on effectiveness of best management practices in improving hydrology and water quality: Needs and opportunities. *Sci. Total Environ.* **2017**, *601–602*, 580–593. [[CrossRef](#)]
20. Sarkar, M.; Pal, S.C.; Islam, A.R.M.T. Groundwater quality assessment for safe drinking water and irrigation purposes in Malda district, Eastern India. *Environ. Earth Sci.* **2022**, *81*, 52. [[CrossRef](#)]
21. Rivera-Rodríguez, D.A.; Beltrán-Hernández, R.I.; Lucho-Constantino, C.A.; Coronel-Olivares, C.; Hernández-González, S.; Villanueva-Ibáñez, M.; Nolasco-Arizmendi, V.; Vázquez-Rodríguez, G.A. Water quality indices for groundwater impacted by geogenic background and anthropogenic pollution: Case study in Hidalgo, Mexico. *Int. J. Environ. Sci. Technol.* **2019**, *16*, 2201–2214. [[CrossRef](#)]
22. Karkhaneh, T.; Sarikhani, R.; Dehnavi, A.G.; Baker, L.L.; Moradpour, A. Controlling factors of groundwater chemistry and statistical analysis of the samples related to ophiolite of Nourabad-Harsin, West of Iran. *Environ. Monit. Assess.* **2022**, *194*, 123. [[CrossRef](#)] [[PubMed](#)]
23. Chen, X.; Jiang, C.; Zheng, L.; Zhang, L.; Fu, X.; Chen, S.; Chen, Y.; Hu, J. Evaluating the genesis and dominant processes of groundwater salinization by using hydrochemistry and multiple isotopes in a mining city. *Environ. Pollut.* **2021**, *283*, 117381. [[CrossRef](#)] [[PubMed](#)]
24. Liu, J.; Peng, Y.; Li, C.; Gao, Z.; Chen, S. An investigation into the hydrochemistry, quality and risk to human health of groundwater in the central region of Shandong Province, North China. *J. Clean. Prod.* **2021**, *282*, 125416. [[CrossRef](#)]
25. Abdulsalam, A.; Ramli, M.F.; Jamil, N.R.; Ashaari, Z.H.; Umar, D.U.A. Hydrochemical characteristics and identification of groundwater pollution sources in tropical savanna. *Environ. Sci. Pollut. Res. Int.* **2022**, *29*, 37384–37398. [[CrossRef](#)]
26. Liu, J.; Gao, Z.; Wang, Z.; Xu, X.; Su, Q.; Wang, S.; Qu, W.; Xing, T. Hydrogeochemical processes and suitability assessment of groundwater in the Jiaodong Peninsula, China. *Environ. Monit. Assess.* **2020**, *192*, 384. [[CrossRef](#)]
27. Apollaro, C.; Di Curzio, D.; Fuoco, I.; Bucciante, A.; Dinelli, E.; Vespasiano, G.; Castrignanò, A.; Rusi, S.; Barca, D.; Figoli, A.; et al. A multivariate non-parametric approach for estimating probability of exceeding the local natural background level of arsenic in the aquifers of Calabria region (Southern Italy). *Sci. Total Environ.* **2022**, *806*, 150345. [[CrossRef](#)]
28. Tyagi, S.; Sarma, K. Expounding major ions chemistry of groundwater with significant controlling factors in a suburban district of Uttar Pradesh, India. *J. Earth Syst. Sci.* **2021**, *130*, 169. [[CrossRef](#)]
29. Chitsazan, M.; Aghazadeh, N.; Mirzaee, Y.; Golestan, Y. Hydrochemical characteristics and the impact of anthropogenic activity on groundwater quality in suburban area of Urmia city, Iran. *Environ. Dev. Sustain.* **2019**, *21*, 331–351. [[CrossRef](#)]
30. Liu, R.-P.; Zhu, H.; Liu, F.; Dong, Y.; El-Wardany, R.M. Current situation and human health risk assessment of fluoride enrichment in groundwater in the Loess Plateau: A case study of Dali County, Shaanxi Province, China. *China Geol.* **2021**, *4*, 487–497. [[CrossRef](#)]
31. Cheng, L.; Si, B.; Wang, Y.; Liu, W. Groundwater recharge mechanisms on the Loess Plateau of China: New evidence for the significance of village ponds. *Agric. Water Manag.* **2021**, *257*, 107148. [[CrossRef](#)]
32. Li, Z.; Coles, A.E.; Xiao, J. Groundwater and streamflow sources in China's Loess Plateau on catchment scale. *Catena* **2019**, *181*, 104075. [[CrossRef](#)]
33. Li, H.X.; Han, S.B.; Wu, X.; Wang, S.; Liu, W.P.; Ma, T.; Zhang, M.N.; Wei, Y.T.; Yuan, F.Q.; Yuan, L. Distribution, characteristics and influencing factors of fresh groundwater resources in the Loess Plateau, China. *China Geol.* **2021**, *4*, 509–526. [[CrossRef](#)]
34. Ling, X.; Ma, J.; Chen, P.; Liu, C.; Horita, J. Isotope implications of groundwater recharge, residence time and hydrogeochemical evolution of the Longdong Loess Basin, Northwest China. *J. Arid Land* **2022**, *14*, 34–55. [[CrossRef](#)]
35. Wang, W.; Li, Z.; Su, H.; Xiao, J.; Han, F.; Li, Z. Spatial and seasonal variability, control factors and health risk of fluoride in natural water in the Loess Plateau of China. *J. Hazard. Mater.* **2022**, *434*, 128897. [[CrossRef](#)]
36. Xiao, J.; Wang, L.; Deng, L.; Jin, Z. Characteristics, sources, water quality and health risk assessment of trace elements in river water and well water in the Chinese Loess Plateau. *Sci. Total Environ.* **2019**, *650*, 2004–2012. [[CrossRef](#)]
37. Zhang, F.; Jin, Z.; Yu, J.; Zhou, Y.; Zhou, L. Hydrogeochemical processes between surface and groundwaters on the northeastern Chinese Loess Plateau: Implications for water chemistry and environmental evolutions in semi-arid regions. *J. Geochem. Explor.* **2015**, *159*, 115–128. [[CrossRef](#)]
38. Gao, Z.; Han, C.; Xu, Y.; Zhao, Z.; Luo, Z.; Liu, J. Assessment of the water quality of groundwater in Bohai Rim and the controlling factors—A case study of northern Shandong Peninsula, north China. *Environ. Pollut.* **2021**, *285*, 117482. [[CrossRef](#)]
39. Li, Y.-Z.; Gao, Z.-J.; Liu, J.-T.; Wang, M.; Han, C. Hydrogeochemical and isotopic characteristics of spring water in the Yarlung Zangbo River Basin, Qinghai-Tibet Plateau, Southwest China. *J. Mt. Sci.* **2021**, *18*, 2061–2078. [[CrossRef](#)]
40. Rajendiran, T.; Sabarathinam, C.; Chandrasekar, T.; Keesari, T.; Senapathi, V.; Sivaraman, P.; Viswanathan, P.M.; Nagappan, G. Influence of variations in rainfall pattern on the hydrogeochemistry of coastal groundwater—An outcome of periodic observation. *Environ. Sci. Pollut. Res.* **2019**, *26*, 29173–29190. [[CrossRef](#)]
41. Manoj, S.; Thirumurugan, M.; Elango, L. Hydrogeochemical modelling to understand the surface water–groundwater interaction around a proposed uranium mining site. *J. Earth Syst. Sci.* **2019**, *128*, 49. [[CrossRef](#)]
42. Wang, Y.; Tong, J.; Hu, B.X.; Dai, H. Combining Isotope and Hydrogeochemistry Methods to Study the Seawater Intrusion: A Case Study in Longkou City, Shandong Province, China. *Water* **2022**, *14*, 789. [[CrossRef](#)]
43. Yu, F.; Zhou, D.; Li, Z.; Li, X. Hydrochemical Characteristics and Hydrogeochemical Simulation Research of Groundwater in the Guohe River Basin (Henan Section). *Water* **2022**, *14*, 1461. [[CrossRef](#)]

44. Liu, J.; Wang, M.; Gao, Z.; Chen, Q.; Wu, G.; Li, F. Hydrochemical characteristics and water quality assessment of groundwater in the Yishu River basin. *Acta Geophys.* **2020**, *68*, 877–889. [[CrossRef](#)]
45. Piper, A.M. A graphic procedure in the geochemical interpretation of water-analyses. *Eos Trans. Am. Geophys. Union* **1944**, *25*, 914–928. [[CrossRef](#)]
46. Qian, H.; Li, P.; Wu, J.; Zhou, Y. Isotopic characteristics of precipitation, surface and ground waters in the Yinchuan plain, Northwest China. *Environ. Earth Sci.* **2012**, *70*, 57–70. [[CrossRef](#)]
47. Liu, J.; Gao, Z.; Wang, M.; Li, Y.; Yu, C.; Shi, M.; Zhang, H.; Ma, Y. Stable isotope characteristics of different water bodies in the Lhasa River Basin. *Environ. Earth Sci.* **2019**, *78*, 71. [[CrossRef](#)]
48. Li, H.; Cheng, X.; Ma, Y.; Liu, W.; Zhou, B. Characteristics and Formation Mechanism of Strontium-rich Groundwater in Malian River Drainage Basin. *Geoscience* **2021**, *35*, 682–692.
49. Gibbs, R.J. Mechanisms Controlling World Water Chemistry. *Science* **1970**, *170*, 1088–1090. [[CrossRef](#)]
50. Xiao, J.; Jin, Z.; Wang, J.; Zhang, F. Major ion chemistry, weathering process and water quality of natural waters in the Bosten Lake catchment in an extreme arid region, NW China. *Environ. Earth Sci.* **2015**, *73*, 3697–3708. [[CrossRef](#)]
51. Wang, Y.; Cheng, X.; Zhang, M. Hydrochemistry and chemical weathering processes of Malian River Basin. *Earth Environ.* **2018**, *46*, 15–22.
52. Craig, H. Isotopic Variations in Meteoric Waters. *Science* **1961**, *133*, 1702–1703. [[CrossRef](#)] [[PubMed](#)]
53. Huang, J.Z.; Tan, H.B.; Wang, R.A.; Wen, X.W. Hydrogen and oxygen isotopic analysis of perennial meteoric water in northwest China. *J. China Hydrol.* **2015**, *35*, 33–39.